NASA TECHNICAL NOTE

NASA TN D-5525

NASA TN D-5525

A METHOD FOR SOLVING HYPERVELOCITY IMPACT PROBLEMS WITH CONSIDERATION OF FREE-SURFACE DISCONTINUITIES

by Richard E. Turner

Langley Research Center
Langley Station, Hampton, Va.

NATIONAL AERONAUTICS AND SPACE ADMINISTRATION • WASHINGTON, D. C. • NOVEMBER 1969

1. Report No. NASA TN D-5525	2. Government Accession No.	3. Recipient's Catalog No.
4. Title and Subtitle A METHOD FOR SOLVING HYPERVELOCITY IMPACT PROBLEMS WITH CONSIDERATION OF FREE-SURFACE DISCONTINUITIES		5. Report Date November 1969 6. Performing Organization Code
7. Author(s) Richard E. Turner		8. Performing Organization Report No. L-6215 10. Work Unit No. 129-03-42-01-23
9. Performing Organization Name and Address NASA Langley Research Center Hampton, Va. 23365		11. Contract or Grant No. 13. Type of Report and Period Covered Technical Note
12. Sponsoring Agency Name and Address National Aeronautics and Space Administration Washington, D.C. 20546		14. Sponsoring Agency Code
15. Supplementary Notes		

16. Abstract

A new method of tracking free surfaces has been developed and used to apply boundary conditions along free-surface discontinuities occurring in the motions of compressible media. The stability of the finite-difference equations used to track those free surfaces has been investigated under simplified conditions and the method was found to be stable.

Also, finite-difference approximations to the continuity equation and general transport equation (which governs the motions of continuous media, in cylindrical coordinates) have been developed in which convective terms are simplified and motion constants (mass, momentum, and internal energy) are conserved in transit.

This system of equations has been applied to the solution of a hypervelocity-impact problem in which an aluminum cylinder with a 10-centimeter base diameter, 8-centimeter top diameter, and 6-centimeter height impacts a 2-centimeter-thick target with a relative velocity of 20 kilometers per second. This solution is compared with an independent solution.

17. Key Words Suggested by Author(s)	18. Distribution Statement
Hypervelocity impact Free-surface discontinuities Eulerian viewpoint	Unclassified – Unlimited

19. Security Classif. (of this report)	20. Security Classif. (of this page)	21. No. of Pages	22. Price*
Unclassified	Unclassified	32	$3.00

*For sale by the Clearinghouse for Federal Scientific and Technical Information
Springfield, Virginia 22151

A METHOD FOR SOLVING HYPERVELOCITY IMPACT PROBLEMS WITH CONSIDERATION OF FREE-SURFACE DISCONTINUITIES

By Richard E. Turner
Langley Research Center

SUMMARY

A new method of tracking free surfaces has been developed and used to apply boundary conditions along free-surface discontinuities occurring in the motions of compressible media. The stability of the finite-difference equations used to track those free surfaces has been investigated under simplified conditions and the method was found to be stable.

Also, finite-difference approximations to the continuity equation and general transport equation (which governs the motions of continuous media, in cylindrical coordinates) have been developed in which convective terms are simplified and motion constants (mass, momentum, and internal energy) are conserved in transit.

This system of equations has been applied to the solution of a hypervelocity-impact problem in which an aluminum cylinder with a 10-centimeter base diameter, 8-centimeter top diameter, and 6-centimeter height impacts a 2-centimeter-thick target with a relative velocity of 20 kilometers per second. This solution is compared with an independent solution.

INTRODUCTION

The acquisition of the scientific knowledge necessary to insure that future spacecraft have adequate (but not excessive) meteoroid shielding will require at least three distinct research approaches. Space-flight experiments are necessary to obtain a limited knowledge of the damage potential of the meteoroid environment. Laboratory impact experiments are necessary to infer the meteoroid environment from the flight meteoroid-damage experiments. Analytical studies of the meteoroid impact-damage phenomena can then be used to complement a limited capability for laboratory impact simulation so that a better knowledge of the damage potential of the meteoroid environment can be obtained and protection against it can be provided.

A variety of digital computer programs have been developed expressly for the purpose of studying these hypervelocity impact problems. Some programs treat the working

media as a compressible fluid, some as elastoplastic solids, and some as perfectly plastic solids. The aim of these calculations is to find crater sizes, deformations on the rear face of finite-thickness targets, and deformations of secondary targets in the case of multiwalled structures. The coordinate viewpoint may be Eulerian, Lagrangian, or Eulerian-Lagrangian mixtures. (For some examples, see ref. 1.)

In programs with the Eulerian viewpoint, the free surfaces of the projectile-target system are treated by diffusion. Discontinuities at the free surfaces are smeared out over several nodal distances. Reference 2 is an example of such a treatment. The "particle in cell" approach (a dual use of Eulerian and Lagrangian viewpoints) also treats the free surfaces by diffusion. Some cases calculated by this approach are presented in reference 3. The method of marker particles is sometimes used to locate free surfaces; however, the marker particles are only visual aids and do not affect the free-surface treatment.

The treatment of free surfaces by diffusion has some disadvantages as well as advantages. Two strong advantages are simplicity and the ability to approximate complex free-surface geometries. Two strong disadvantages are that boundary conditions cannot be applied accurately and the position of the free surfaces cannot be defined accurately.

A method for tracking free surfaces is given here which can be used to apply boundary conditions along the free surface of a system provided the slope of the free surface is finite everywhere. A mass transport equation and a general transport equation are derived in the Eulerian frame of reference from an intuitive basis. These transport equations represent a simple treatment of the convectivelike terms in a continuum and yield smooth space solutions to the finite-difference equations.

The model used to represent the target-projectile medium is a compressible nonconducting fluid with a spherical stress tensor. (See ref. 4.)

SYMBOLS

A,B	time-dependent coefficients in a Fourier series, centimeters/second
a,b	sgn(-u), sgn(-w), dimensionless
C	time-dependent coefficient in a Fourier series, centimeters
E	internal energy per unit mass, ergs/gram
f,g	equations of state

H	damping constant, dimensionless
M	amplification matrix appearing in numerical stability studies, dimensionless
p	pure hydrostatic pressure, dynes/centimeter^2
Q	arbitrary quantity being transported, dimensions arbitrary
q	artificial viscosity used to generate entropy, dynes/centimeter^2
r	radius, centimeters
$S(\rho)$	density source, $\frac{\text{grams/centimeter}^3}{\text{second}}$
$S(\rho E)$	energy source, $\frac{\text{ergs/centimeter}^3}{\text{second}}$
$S(\rho Q)$	source for arbitrary quantity Q being transported, $\frac{(\text{grams/centimeter}^3)(Q \text{ dimensions})}{\text{second}}$
$S(\rho u), S(\rho w)$	sources for momentum, $\frac{\text{grams/centimeter}^2}{\text{second}^2}$
s	displacement along a free surface, centimeters
t	time, seconds
U	radial-velocity disturbance, centimeters/second
u	radial velocity, centimeters/second
V	velocity, centimeters/second
W	longitudinal-velocity disturbance, centimeters/second
w	longitudinal velocity, centimeters/second
x	specified radial position, centimeters
z	longitudinal coordinate, centimeters

β	space translation, centimeters
γ	Fourier exponent used in numerical stability study, centimeter^{-1}
δ	elemental volume in cylindrical coordinates, centimeters^3
Θ	angular variable in cylindrical coordinates, radians
θ	angle between the free surface and a constant-z parametric line, radians
λ	eigenvalues of a square matrix, dimensionless
ξ	specified radial position, centimeters
ρ	density, grams/centimeter^3
σ	pure tensile stress, dynes/centimeter^2
τ	time increment, seconds
Φ	free-surface-coordinate disturbance, centimeters
ϕ	free-surface coordinate, centimeters
ψ	state variable for target-projectile system, arbitrary

Subscripts:

B	evaluated along a free surface
j	radial coordinate $j\Delta r$
k	longitudinal coordinate $k\Delta z$

Superscript:

l	time $l\tau$

Notations:

$[\ ]$	square matrix

$\{\}$ column vector

$|\ |$ Euclidean norm, dimensions arbitrary

The operator $d(\ )/dt$ denotes time derivative following the particle (comoving). A bar over a symbol denotes a vector.

ANALYSIS

The problem to be solved concerns a solid circular cylinder impacting a solid target of finite thickness. The pressure generated by the impact is assumed to be sufficiently high to allow yield strengths to be neglected. The resulting medium can be approximated by a compressible fluid.

Differential Equations of Motion For Compressible Nonconducting Fluids With Pure Hydrostatic Stress

The differential equations of motion for compressible fluids with pure hydrostatic stress are (from ref. 4) the momentum equation

$$\rho \frac{d\overline{V}}{dt} = \nabla\sigma \tag{1}$$

the energy equation

$$\rho \frac{dE}{dt} = -\frac{\sigma}{\rho}\frac{d\rho}{dt} \tag{2}$$

and the continuity equation

$$\frac{d\rho}{dt} = -\rho\left(\nabla \cdot \overline{V}\right) \tag{3}$$

where ρ is mass density, $\overline{V}$ is velocity, σ is stress, E is internal energy per unit mass, t is time, $d(\ )/dt$ is the comoving time derivative of $(\ )$, and ∇ is the classical vector del operator. The operator $d(\ )/dt$ is given by

$$\frac{d(\ )}{dt} = \frac{\partial(\ )}{\partial t} + \overline{V} \cdot \nabla(\ ) \tag{4}$$

where $\partial(\ )/\partial t$ is the time derivative of $(\ )$ for fixed-space coordinates. The algebraic equations needed to complete the description of compressible fluids with pure hydrostatic stress are the constitutive equation

$$\sigma = -(p + q) \tag{5}$$

where p and q are nonnegative, and the equation of state

$$p = f(E,\rho) \tag{6}$$

In these equations p is hydrostatic pressure and q is an artificial viscosity term which is introduced for entropy production in such things as shock waves. (See ref. 4.)

Interior Equations of Motion in Finite-Difference Form

If r is the radial coordinate, z is the longitudinal coordinate, u is the radial velocity component, w is the longitudinal velocity component, Δ denotes a coordinate increment, the superscript l refers to time $l\tau$, the subscript j refers to the radial coordinate $j\Delta r$, k refers to the longitudinal coordinate $k\Delta z$, and the fraction 1/2 in subscripts refers to values averaged from interval end points, then from appendix A the equations of motion for the medium can be written as the transport equation

$$\rho^{l}_{j,k} \frac{\partial Q^{l}_{j,k}}{\partial t} = -a\, \rho^{l}_{j+(a/2),k}\, u^{l}_{j+(a/2),k} \frac{Q^{l}_{j+a,k} - Q^{l}_{j,k}}{\Delta r} - b\, \rho^{l}_{j,k+(b/2)}\, w^{l}_{j,k+(b/2)} \frac{Q^{l}_{j,k+b} - Q^{l}_{j,k}}{\Delta z}$$

$$- \rho^{l}_{j+(a/2),k}\, u^{l}_{j+(a/2),k} \frac{Q^{l}_{j+a,k} - Q^{l}_{j,k}}{2r_j} + S(\rho Q)^{l}_{j,k} - \tau \frac{\partial \rho^{l}_{j,k}}{\partial t} \frac{\partial Q^{l}_{j,k}}{\partial t} \tag{7}$$

where Q assumes the role of E, u, and w, and where a is $\operatorname{sgn}(-u)$ and b is $\operatorname{sgn}(-w)$. The source equations are

$$S(\rho u)^{l}_{j,k} = \frac{\sigma^{l}_{j+(1/2),k} - \sigma^{l}_{j-(1/2),k}}{\Delta r} \tag{8}$$

$$S(\rho w)^{l}_{j,k} = \frac{\sigma^{l}_{j,k+(1/2)} - \sigma^{l}_{j,k-(1/2)}}{\Delta z} \tag{9}$$

$$S(\rho E)^{l}_{j,k} = -\frac{\sigma^{l}_{j,k}}{\rho^{l}_{j,k}} \frac{d\rho^{l}_{j,k}}{dt} \tag{10}$$

along with the continuity equation

$$\frac{\partial \rho^{l}_{j,k}}{\partial t} + a\, u^{l}_{j+(a/2),k} \frac{\rho^{l}_{j+a,k} - \rho^{l}_{j,k}}{\Delta r} + b\, w^{l}_{j,k+(b/2)} \frac{\rho^{l}_{j,k+b} - \rho^{l}_{j,k}}{\Delta z} + u^{l}_{j+(a/2),k} \frac{\rho^{l}_{j+a,k} - \rho^{l}_{j,k}}{2r_j}$$

$$= -\rho^{l}_{j,k} \frac{u^{l}_{j+(1/2),k} - u^{l}_{j-(1/2),k}}{\Delta r} - \rho^{l}_{j,k} \frac{w^{l}_{j,k+(1/2)} - w^{l}_{j,k-(1/2)}}{\Delta z} - \rho^{l}_{j,k} \frac{u^{l}_{j+(1/2),k} + u^{l}_{j-(1/2),k}}{2r_j} \tag{11}$$

and

$$\frac{d\rho^{l}_{j,k}}{dt} = \frac{\partial \rho^{l}_{j,k}}{\partial t} + a\, u^{l}_{j+(a/2),k} \frac{\rho^{l}_{j+a,k} - \rho^{l}_{j,k}}{\Delta r} + b\, w^{l}_{j,k+(b/2)} \frac{\rho^{l}_{j,k+b} - \rho^{l}_{j,k}}{\Delta z}$$

$$+ u^{l}_{j+(a/2),k} \frac{\rho^{l}_{j+a,k} - \rho^{l}_{j,k}}{2r_j} \tag{12}$$

From reference 5, the equation of state for aluminum, valid to about 5×10^{12} dynes/centimeter^2, is

$$p(E,\rho) = \left(0.5 + \frac{1.63}{\frac{E \times 10^{-12}}{0.05\left(\frac{\rho}{2.7}\right)^2} + 1}\right) E\rho + 0.752 \times 10^{12}\left(\frac{\rho}{2.7} - 1\right) + 0.65 \times 10^{12}\left(\frac{\rho}{2.7} - 1\right)^2$$

if $p \geq 0$. If the equation yields negative values, p is taken as zero.

The damping term q, which is introduced to render the numerical solution stable and give structure to the shock wave (see ref. 4) is

$$q = \frac{H\left(\Delta r^2 + \Delta z^2\right)}{\rho} \left|\frac{d\rho}{dt}\right| \frac{d\rho}{dt} \tag{13}$$

where H is a constant which is chosen by trial and error. The value for H used here was 5 for $\frac{d\rho}{dt} \geq 0$; otherwise H is zero.

Boundary Considerations

Equations (7) to (12) can be solved in a straightforward manner if the fluid medium occupies a simple cylindrical region. In the problem considered here the fluid medium occupies a region which has little resemblance to a cylinder. The approach often used to

circumvent this difficulty is to surround the interior region with a cylindrical region. The region between the problem boundary and cylindrical boundary is then assumed to be a vacuum. (See fig. 1.) As time increases, the projectile moves into the target region and both regions become distorted and spill into the empty regions. In taking differences along the free surfaces, the discontinuities in the system properties are ignored. Here, along the free surfaces, the requirement for smooth solutions and the simultaneous requirement for free-surface definition meet in conflict. Smooth solutions require that short-wavelength space variations be attenuated while good free-surface definition requires that short-wavelength space variations be maintained. This incompatibility between smoothness and free-surface definition can be eliminated by tracking the free surfaces and taking the boundary discontinuities into considerations near the free surfaces.

Free-Surface Equations of Motion

Consider the surface of revolution shown in figure 2, which separates the interior from the void region. This surface can be tracked by tracking the intersection of the surface of revolution with the vertical parametric lines of constant radial coordinate. Let ϕ be the distance along a vertical parametric line to the surface of revolution, so that

$$\phi = \phi(r,t) \tag{14}$$

It is seen from figure 3 that

$$\phi(x, t+\tau) = \phi(\xi,t) + w\tau \tag{15}$$

Let $\Delta\phi$ be $\phi(x, t+\tau) - \phi(x,t)$; then equation (15) is equivalent to

$$\Delta\phi = w\tau - \frac{\phi(x,t) - \phi(\xi,t)}{x - \xi} \frac{x - \xi}{\tau} \tau \tag{16}$$

and since $x - \xi$ equals $u\tau$, equation (16) can be divided by τ to get

$$\frac{\Delta\phi}{\tau} = w - u \frac{\phi(x,t) - \phi(\xi,t)}{x - \xi} \tag{17}$$

Now make the approximation that τ tends to zero, and transform equation (17) to the index notation to get

$$\frac{\partial \phi_j^l}{\partial t} = w_{j,B}^l - a u_{j,B}^l \frac{\phi_{j+a}^l - \phi_j^l}{\Delta r} \tag{18}$$

Since ϕ_j^l will not, in general, coincide with any of the system's interior points, equation (18) introduces two quantities to keep track of: $u_{j,B}^l$ and $w_{j,B}^l$. Equations for these quantities can be developed from equations (1) to (6). Two approaches will be given for computing $u_{j,B}^l$ and $w_{j,B}^l$.

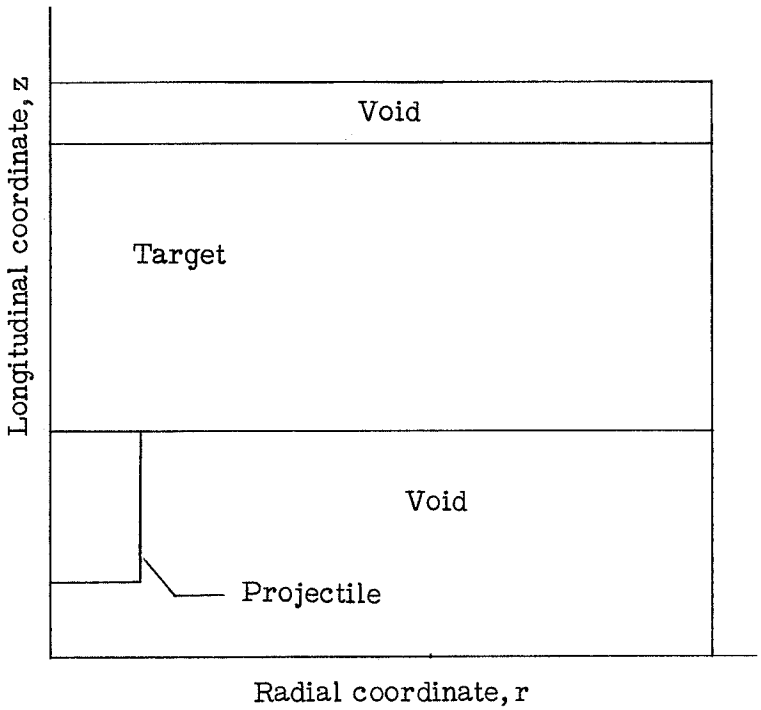

Figure 1.- Typical initial geometry of an impact problem.

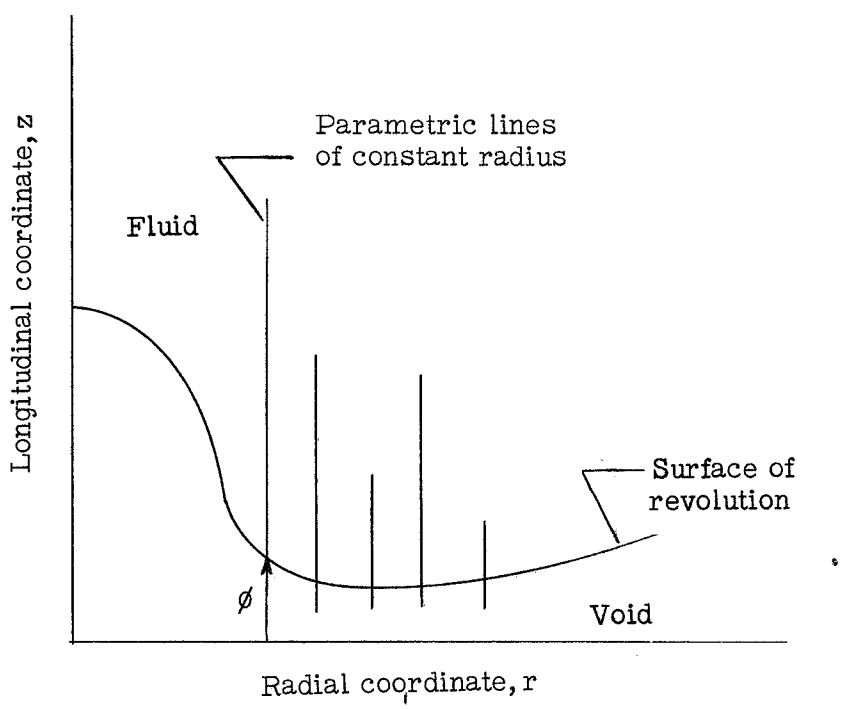

Figure 2.- Typical surface of revolution intersecting the parametric lines of constant radius in cylindrical coordinates.

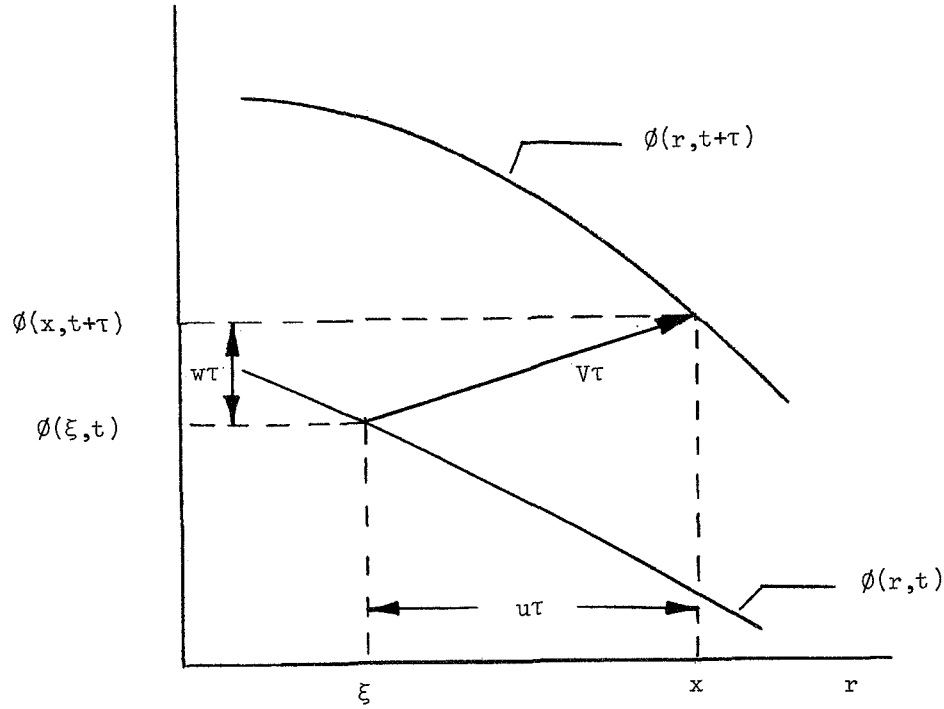

Figure 3.- Motion of surface of revolution relative to the vertical lines of constant radius.

First approach.- Along the free surface, σ is zero. From equation (5), along the free surface,

$$\sigma = -(p + q) = 0$$

Thus, since p and q are nonnegative,

$$p(\text{Boundary, } t) = q(\text{Boundary, } t) = 0$$

Equation (2) shows that

$$\frac{dE}{dt}(\text{Boundary, } t) = 0$$

so that

$$E(\text{Boundary, } t) = 0$$

The equation of state, equation (6), can be inverted to give

$$\rho = g(p,E)$$

Since $p = E = 0$ along the free surfaces,

$$\rho(\text{Boundary, } t) = g(0,0) = \text{Constant} \tag{19}$$

Equation (1) can now be used to find the two other equations needed for $u^{l}_{j,B}$ and $w^{l}_{j,B}$.

Consider figure 3 for a particle on the free surface, moving with the free surface. The identity

$$\overline{V}(x,\ t+\tau) - \overline{V}(\xi,t) \equiv \left[\overline{V}(x,\ t+\tau) - \overline{V}(x,t)\right] + \left[\overline{V}(x,t) - \overline{V}(\xi,t)\right] \tag{20}$$

can be written, and the following equation can be derived in a manner similar to that in appendix B:

$$\frac{\left[\Delta\overline{V}\left(\frac{x+\xi}{2},\ t+\frac{\tau}{2}\right)\right]_{\text{trajectory}}}{\tau} = \frac{\left[\Delta\overline{V}\left(x,\ t+\frac{\tau}{2}\right)\right]_{\text{time}}}{\tau} + \frac{\overline{V}(x,t) - \overline{V}(\xi,t)}{x - \xi}\frac{x - \xi}{\tau} \tag{21}$$

As in appendix B, the approximation is made that τ tends to zero. Equation (21) is changed to index notation to get

$$\frac{d\overline{V}^{l}_{j,B}}{dt} = \frac{\partial\overline{V}^{l}_{j,B}}{\partial t} + au^{l}_{j,B}\frac{\overline{V}^{l}_{j+a,B} - \overline{V}^{l}_{j,B}}{\Delta r} \tag{22}$$

This expression is the comoving derivative of a point on the surface, and thus z is not an independent variable, but $z = \phi(r,t)$.

When equation (22) is combined with equation (1), there follows

$$\frac{\partial u^{l}_{j,B}}{\partial t} = -au^{l}_{j,B}\frac{u^{l}_{j+a,B} - u^{l}_{j,B}}{\Delta r} + \frac{1}{\rho^{l}_{j,B}}\frac{\partial\sigma^{l}_{j,B}}{\partial r} \tag{23}$$

and

$$\frac{\partial w^{l}_{j,B}}{\partial t} = -au^{l}_{j,B}\frac{w^{l}_{j+a,B} - w^{l}_{j,B}}{\Delta r} + \frac{1}{\rho^{l}_{j,B}}\frac{\partial\sigma^{l}_{j,B}}{\partial z} \tag{24}$$

Values for $\frac{\partial\sigma^{l}_{j,B}}{\partial r}$ and $\frac{\partial\sigma^{l}_{j,B}}{\partial z}$ can be found by noticing that

$$\frac{\partial\sigma^{l}_{j,B}}{\partial s} = \frac{\partial\sigma^{l}_{j,B}}{\partial z}\sin\theta + \frac{\partial\sigma^{l}_{j,B}}{\partial r}\cos\theta = 0$$

where s is a displacement along the free surface and θ is the angle measured from the horizontal to the free surface in figure 4. The partial derivative of $\sigma^{l}_{j,B}$ with respect to z is

$$\frac{\partial\sigma^{l}_{j,B}}{\partial z} = \frac{\sigma^{l}_{j,k}}{k\Delta z - \phi^{l}_{j}} \tag{25}$$

where $\sigma^{l}_{j,k}$ is evaluated at the closest interior point. Now solving for $\frac{\partial \sigma^{l}_{j,B}}{\partial r}$ from $\frac{\partial \sigma^{l}_{j,B}}{\partial s}$ and letting

$$\tan \theta = \frac{\phi^{l}_{j+1} - \phi^{l}_{j-1}}{2\Delta r}$$

yields

$$\frac{\partial \sigma^{l}_{j,B}}{\partial r} = - \frac{\sigma^{l}_{j,k}\left(\phi^{l}_{j+1} - \phi^{l}_{j-1}\right)}{\left(k\Delta z - \phi^{l}_{j}\right)2\Delta r} \tag{26}$$

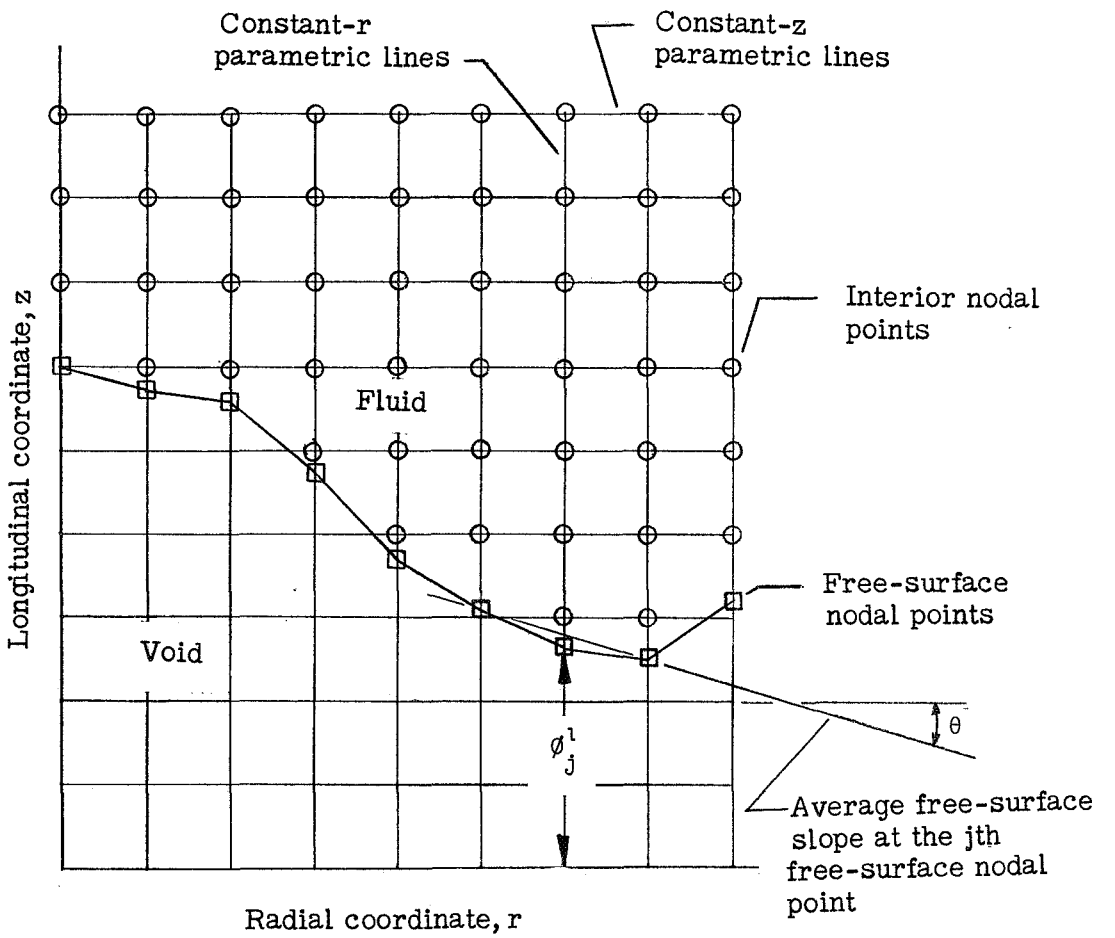

Figure 4.- Free-surface coordinates in relation to the fluid interior nodal points.

Second approach.- In the second approach equations (23) and (24) are still valid, but an equation for $\frac{\partial \rho^{l}_{j,B}}{\partial t}$ is obtained from equation (22) by replacing $\overline{V}^{l}_{j,B}$ with $\rho^{l}_{j,B}$ to get

$$\frac{d\rho^{l}_{j,B}}{dt} = \frac{\partial \rho^{l}_{j,B}}{\partial t} + au^{l}_{j,B} \frac{\rho^{l}_{j+a,B} - \rho^{l}_{j,B}}{\Delta r} \tag{27}$$

An equation for $\frac{d\rho^{l}_{j,B}}{dt}$ is obtained by noticing that the left-hand side of equation (A4) is equal to $\frac{d\rho^{l}_{j,B}}{dt}$, and taking the limit of the right-hand side as Δr and Δz tend to zero. The result is

$$\frac{d\rho^{l}_{j,B}}{dt} = -\rho^{l}_{j,B}\left(\frac{\partial u^{l}_{j,B}}{\partial r} + \frac{\partial w^{l}_{j,B}}{\partial z} + \frac{u^{l}_{j,B}}{r_j}\right) \tag{28}$$

Now let

$$\frac{\partial u^{l}_{j,B}}{\partial s} = \frac{u^{l}_{j+1,B} - u^{l}_{j-1,B}}{\Delta s} \tag{29}$$

$$\frac{\partial w^{l}_{j,B}}{\partial z} = \frac{w^{l}_{j,B} - w^{l}_{j,k}}{\phi^{l}_{j} - k\Delta z} \tag{30}$$

$$\frac{\partial u^{l}_{j,B}}{\partial z} = \frac{u^{l}_{j,B} - u^{l}_{j,k}}{\phi^{l}_{j} - k\Delta z} \tag{31}$$

and

$$\tan \theta = \frac{\phi^{l}_{j+1} - \phi^{l}_{j-1}}{2\Delta r} \tag{32}$$

Then, since

$$\frac{\partial u^{l}_{j,B}}{\partial s} = \frac{\partial u^{l}_{j,B}}{\partial r} \cos \theta + \frac{\partial u^{l}_{j,B}}{\partial z} \sin \theta \tag{33}$$

solving for $\frac{\partial u^{l}_{j,B}}{\partial r}$ from equation (33) and substituting from equations (29) to (32) gives

$$\frac{\partial u^{l}_{j,B}}{\partial r} = \frac{u^{l}_{j+1,B} - u^{l}_{j-1,B}}{2\Delta r} - \frac{\left(u^{l}_{j,B} - u^{l}_{j,k}\right)\left(\phi^{l}_{j+1} - \phi^{l}_{j-1}\right)}{\left(\phi^{l}_{j} - k\Delta z\right)2\Delta r} \tag{34}$$

Equations (27), (28), (30), and (34) define $\frac{\partial \rho^{l}_{j,B}}{\partial t}$ in terms of known quantities.

Application of Boundary Conditions

Figure 5 shows a target-projectile system during the time of crater formation. The front free surface and rear free surface are in continual motion and can be tracked by the use of free-surface coordinates. The center-line boundary is fixed and its associated boundary conditions can be applied easily.

Along the center-line boundary, boundary conditions can be applied by a fictitious column of nodal points on the opposite side of the longitudinal axis, each point being a mirror-image nodal point, and $u^{l}_{j,k} = 0$.

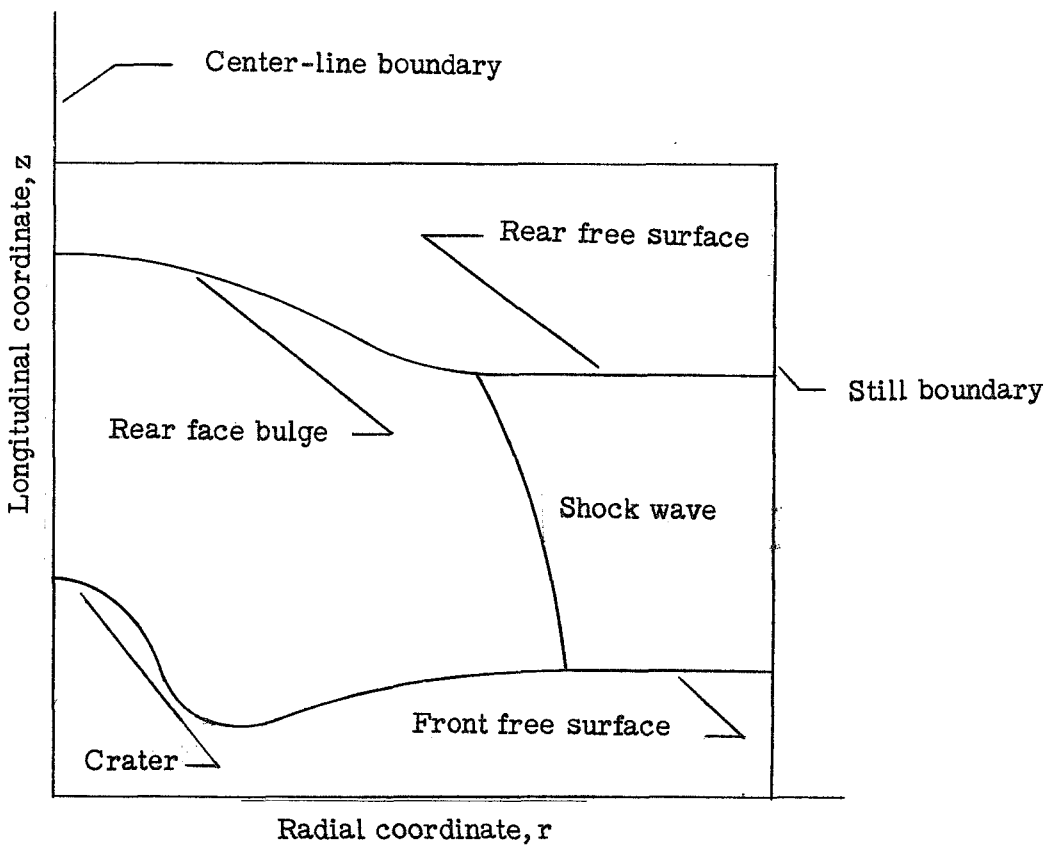

Figure 5.- Typical boundaries of target-projectile system during impact.

Boundary conditions along the free surfaces can be applied by assigning such property values to nodal points (adjacent to, but outside, the free surfaces) that the property values vary linearly from inside nodal points to outside nodal points and pass through the required free-surface values.

Numerical Computation Cycle

The dependent interior variables governing the fluid motions are $u^l_{j,k}$, $w^l_{j,k}$, $E^l_{j,k}$, and $\rho^l_{j,k}$ and their governing equations are equations (7), (8), (9), (10), and (11). The hydrostatic stress $\sigma^l_{j,k}$ is calculated from equation (13) and the equation of state.

For the first approach, the dependent variables governing the motion of the free surfaces are ϕ^l_j, $u^l_{j,B}$, $w^l_{j,B}$, and $\rho^l_{j,B}$, and their respective governing equations are equations (18), (23), and (24) and constant density along the free surfaces.

The second approach is the same as the first approach except that $\frac{\partial \rho^l_{j,B}}{\partial t}$ is calculated from equations (27), (28), (30), and (34).

The stress derivatives are calculated from equations (25) and (26).

When all the dependent variables $\psi^l_{j,k}$ are specified at time t, the governing equations and boundary conditions are used to calculate $\frac{\partial \psi^l_{j,k}}{\partial t}$ at time t. The values of the dependent variables at time $t + \tau$ can then be found by use of the first two terms of a Taylor series:

$$\psi^{l+1}_{j,k} = \psi^l_{j,k} + \frac{\partial \psi^l_{j,k}}{\partial t} \tau \tag{35}$$

Numerical Stability of the Free-Surface Coordinates

A study of the stability of the equations governing the fluid interior motion can be found in the literature; for example, see reference 4. A complete study of the stability of the free-surface equations is beyond the scope of this report; however, when the free-surface equations are uncoupled from the interior flow (for the boundary treatment in the first approach) a study of their stability becomes tractable and is given in appendix C.

NUMERICAL EXAMPLE

Equations (7), (8), (9), (10), (11), (18), (23), and (24) were programed for the digital computer, and the results of a test case treated by the first approach are compared with the solution of a similar problem taken from reference 3.

The criteria used to evaluate the status and property values of nodal points exterior to the problem region are:

(1) Nodal points closer to the free surfaces than $\Delta z/2$ vertically or $\Delta r/2$ horizontally, as well as nodal points on the void side of the free surface, are considered to be exterior to the problem region.

(2) Exterior nodal points adjacent to interior nodal points have such property values assigned to them that the boundary conditions are linearly satisfied.

The test case simulates an aluminum truncated cone striking an aluminum target with an impact velocity of 20×10^5 cm/sec. The top diameter of the projectile is 8 centimeters, the base diameter is 10 centimeters, and the height is 6 centimeters. The target is 2 centimeters thick.

The case of reference 3 simulates an aluminum cylinder striking an aluminum target with an impact velocity of 20×10^5 cm/sec. The cylinder diameter is 10 centimeters and the height is 10 centimeters. The target is 2 centimeters thick.

The initial differences between the two problems are the sloping wall and shortened height of the test-case projectile. The sloping wall is necessary because infinite free-surface slopes cannot be accommodated by the equations derived herein. The difference in height of the two projectiles is inconsequential because at the time of comparison the rearward-traveling shock wave has not reached the rear free surface of the projectile.

Figure 6 shows the projectile and target at impact. The direction of travel of the projectile is along the longitudinal coordinate into the target.

Figure 7 shows the geometry of the two solutions 2.56 microseconds after impact. The dashed line represents the solution from reference 3 and the solid line represents the test-case solution. The most obvious difference between the solutions is the area inside the free surfaces. Since the solution from reference 3 accounts for the free surfaces by diffusion of material into empty cells, it is to be expected that the free surfaces of the test case should be contained inside the free surfaces of reference 3, as is shown in figure 7.

Figure 8 shows property variations along the center line. The velocity variations are shown in figure 8(a), density variations are shown in 8(b), and hydrostatic-stress variations are shown in 8(c).

At the time of comparison, the shock wave traveling into the target has already encountered the target rear surface and the accompanying expansion wave has reentered the target and has overtaken the shock wave traveling into the projectile. The shock wave traveling into the projectile is situated at about $z = 7$ centimeters.

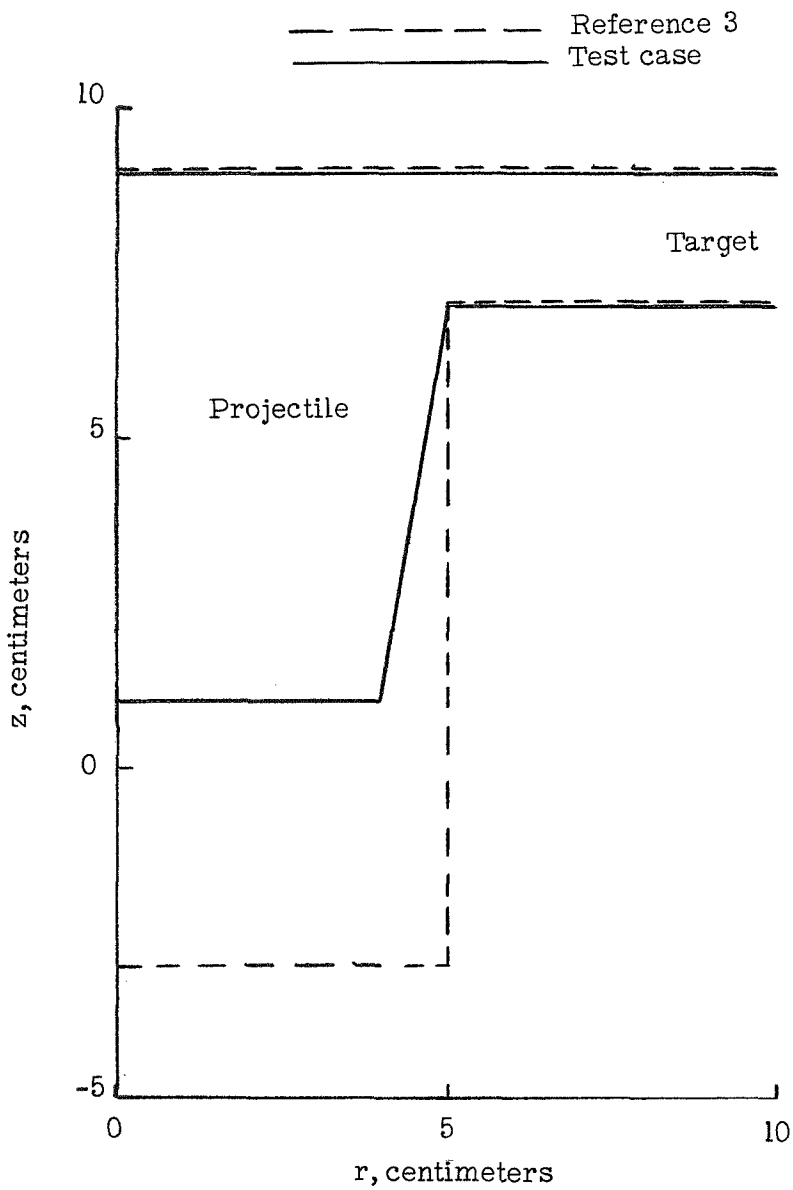

Figure 6.- Target-projectile system at impact.

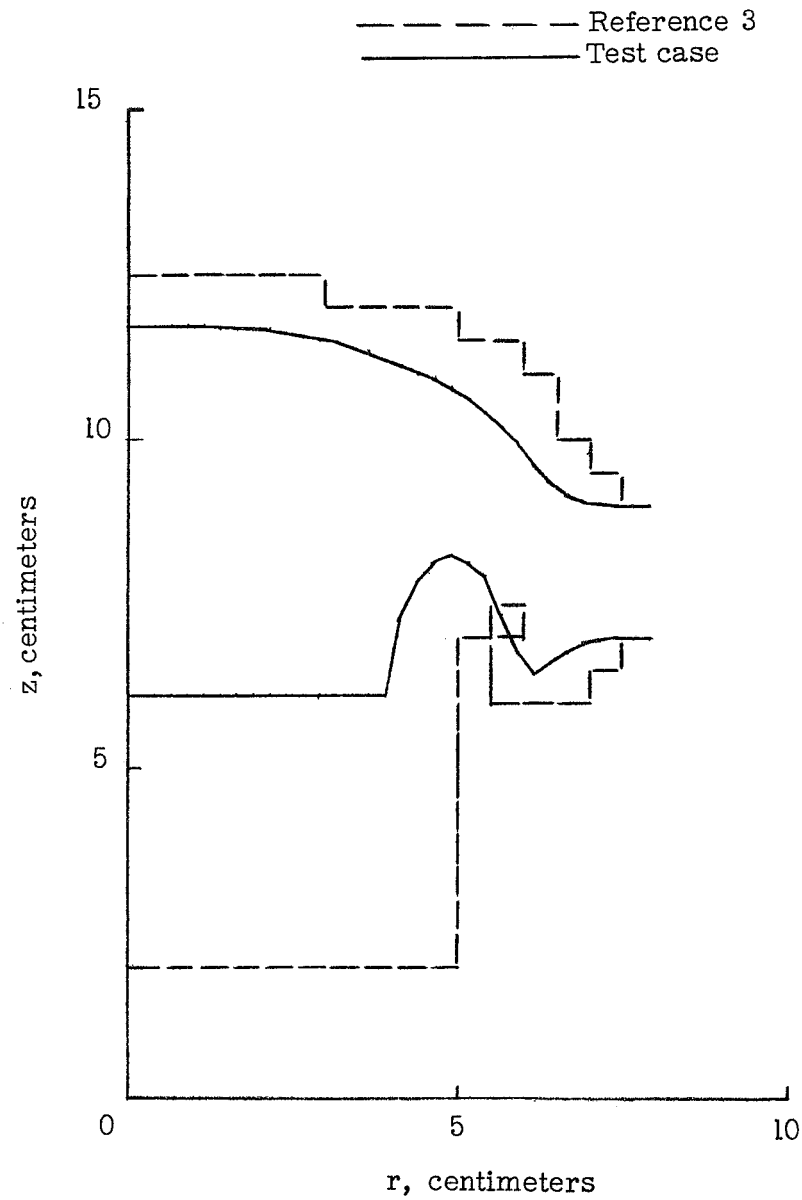

Figure 7.- Geometry of target-projectile system 2.56 microseconds after impact.

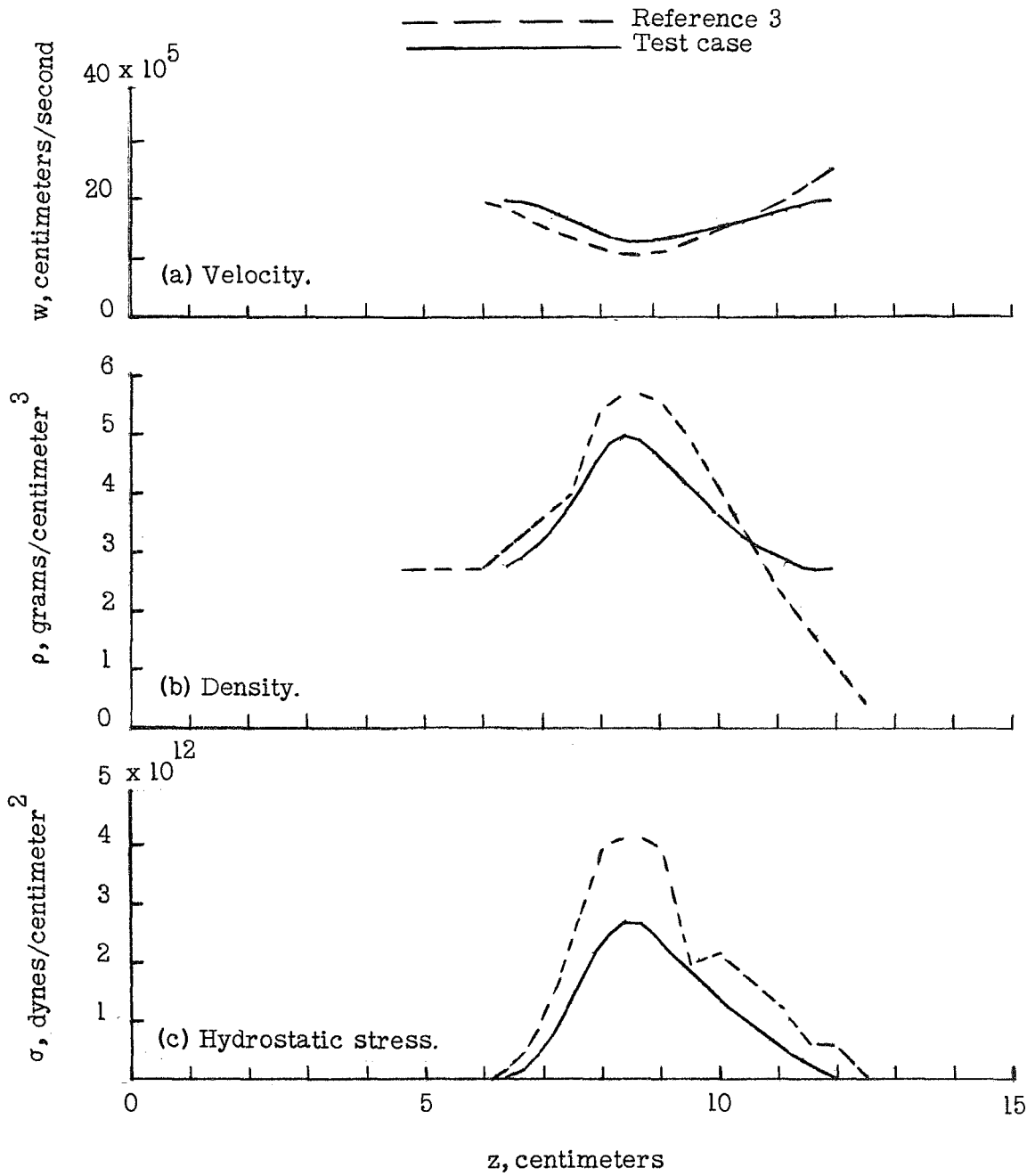

Figure 8.- Properties of target-projectile system along center-line coordinate 2.56 microseconds after impact.

The velocity variations shown in figure 8(a) are in fair agreement. The material approaching the shock wave is being decelerated from its original speed of 20×10^5 cm/sec. The material past the shock wave is being accelerated by the expansion wave from the rear free surface of the target.

The density variations shown in figure 8(b) differ somewhat. The test-case density is lower (at the shock-wave location) than the density from reference 3 because of the value of H used in equation (13). Independent one-dimensional computations were performed to determine a value of H which would give smooth property variations, and a value of 5 was chosen. A smaller value of H would have resulted in a higher density peak for the test case. This dependence of property variations on H because of the small number of nodal points in the target has been indicated by several independent computer runs. For a smaller number of nodal points in the target, the dependence of property values on H is increased. The shape of the density curves near the free surface of the target differs appreciably. This difference is caused by the different methods of treating free surfaces.

The stress curves shown in figure 8(c) are similar in shape but the solution of reference 3 is higher than the test-case solution by about 10^{12} dynes/cm^2. This is thought to be caused by the value of H used in equation (13), as the peak stress, like the peak density, has been found to be a function of H. The stress curve for z less than 8 centimeters represents the shock wave traveling into the projectile and the stress curve for z greater than 8 centimeters represents the expansion wave overtaking the shock wave. The shock wave is about 2 centimeters thick in this case, far thicker than a real shock wave. This thickness is caused by the term q. A smaller value of H in equation (13) corresponds to thinner shock waves, and a larger value of H corresponds to thicker shock waves.

The second approach was also programed (allowing for variable density along the free surfaces) and a computer run was made for the same initial conditions as were used with the first approach. The results with the second approach were nearly identical to those with the first approach except for density variations near the free surfaces. The different densities predicted by the two methods are presented in figure 9.

Along the center line (fig. 9(a)) the density distributions are seen to be the same except near the rear free surface, where the second approach yields slightly lower values than the first approach. Figures 9(b) and 9(c) show density variations along the front and rear free surfaces, respectively. The curves from the second approach show small density increases at the positions where the radially traveling shock wave is interacting with the free surfaces, and small density decreases behind the shock wave.

In choosing between the first and second approach, it should be noted that the shock-wave smearing and the adiabatic energy equation (no heat conduction) used herein are

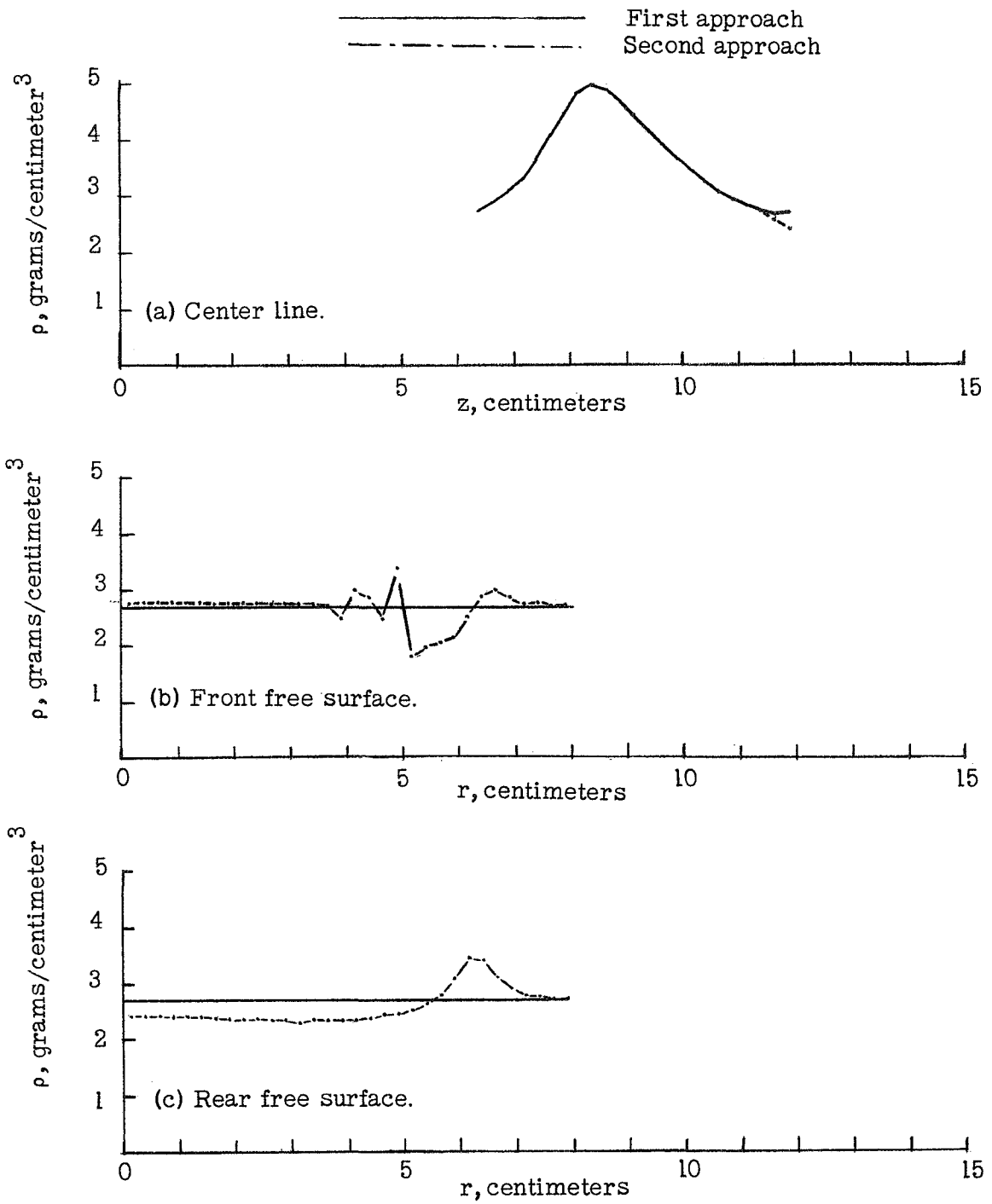

Figure 9.- Density variations for the second approach compared with the first approach.

responsible for the constant free-surface density in the first approach and for the small density variations along the free surfaces in the second approach. Since the energy equation is adiabatic, no mechanism is available to bring heat to the free surface to cause expansion; furthermore, the shock-wave smearing decreases property gradients so drastically that no appreciable heat could be transferred to the free surfaces even if heat conduction terms were included in the energy equation.

The first approach is mathematically correct for the working media considered and it is simpler to use than the second approach.

The roughness in the density variation with the second approach for r between 4 and 5 centimeters, shown in figure 9(b), is thought to be caused by the integration scheme used here. More computer runs have shown that this roughness can be eliminated by a small amount of smoothing of the data (a suitable weighting of the density at each point with its two nearest neighbors).

CONCLUDING REMARKS

A method of tracking free surfaces has been developed. Also, finite-difference approximations to the continuity equation and general transport equation have been derived in which the convective terms are simplified and mass, momentum, and internal energy are conserved in transit. The resulting fluid motions calculated by finite differences did not exhibit obvious instabilities. Two different methods are given for computing density variations along the free surfaces.

Langley Research Center,
National Aeronautics and Space Administration,
Langley Station, Hampton, Va., August 27, 1969.

APPENDIX A

FINITE-DIFFERENCE APPROXIMATION FOR THE TRANSPORT EQUATIONS IN CYLINDRICAL COORDINATES

Consider the elemental volume δ_j in figure 10, where

$$\delta_j = \int_0^{2\pi} r_j \, \Delta r \, \Delta z \, d\Theta = 2\pi r_j \, \Delta r \, \Delta z$$

and consider the density $\rho^l_{j,k}$ of a fluid flowing through δ_j at

$$t = l\tau$$

$$r = j\Delta r$$

$$z = k\Delta z$$

The conservation of mass flowing through δ_j requires that

$$\delta_j \frac{\partial \rho^l_{j,k}}{\partial t} + 2\pi \, r_{j+(1/2)} \, u^l_{j+(1/2),k} \, \rho^l_{j+(1/2),k} \, \Delta z - 2\pi \, r_{j-(1/2)} \, u^l_{j-(1/2),k} \, \rho^l_{j-(1/2),k} \, \Delta z$$

$$+ 2\pi \, r_j \, w^l_{j,k+(1/2)} \, \rho^l_{j,k+(1/2)} \, \Delta r - 2\pi \, r_j \, w^l_{j,k-(1/2)} \, \rho^l_{j,k-(1/2)} \, \Delta r = S(\rho)^l_{j,k} \, \delta_j \qquad \text{(A1)}$$

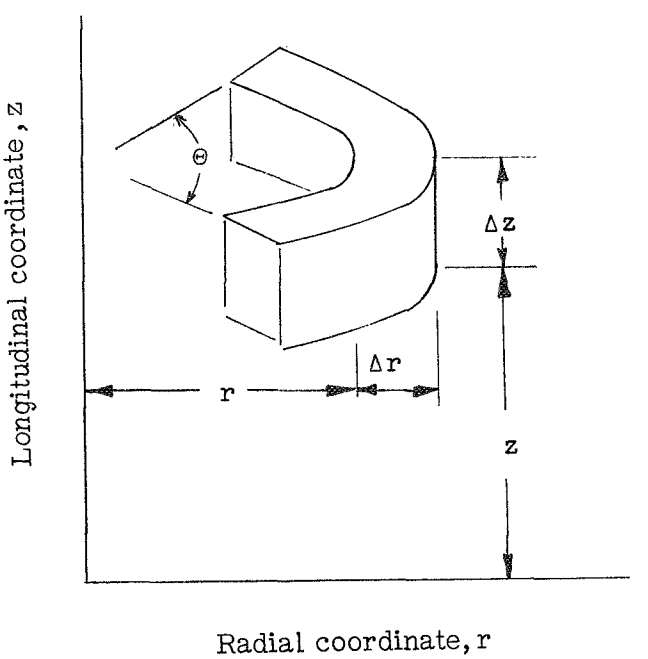

Figure 10.- Elemental volume in cylindrical coordinates.

where u is the radial velocity component, w is the longitudinal velocity component, and $S(\rho)$ is a mass source per unit volume. From both sides of equation (A1) subtract the quantity

$$2\pi\, r_{j+(1/2)} \rho^{l}_{j,k}\, u^{l}_{j+(1/2),k} \Delta z - 2\pi\, r_{j-(1/2)}\, \rho^{l}_{j,k}\, u^{l}_{j-(1/2),k}\, \Delta z$$

$$+ 2\pi\, r_j\, \rho^{l}_{j,k}\, w^{l}_{j,k+(1/2)}\, \Delta r - 2\pi\, r_j\, \rho^{l}_{j,k}\, w^{l}_{j,k-(1/2)}\, \Delta r$$

and after some rearrangement get

$$\delta_j \frac{\partial \rho^{l}_{j,k}}{\partial t} + 2\pi\, r_{j+(1/2)}\, u^{l}_{j+(1/2),k}\left(\rho^{l}_{j+(1/2),k} - \rho^{l}_{j,k}\right)\Delta z$$

$$+ 2\pi\, r_{j-(1/2)}\, u^{l}_{j-(1/2),k}\left(\rho^{l}_{j,k} - \rho^{l}_{j-(1/2),k}\right)\Delta z + 2\pi\, r_j\, w^{l}_{j,k+(1/2)}\left(\rho^{l}_{j,k+(1/2)} - \rho^{l}_{j,k}\right)\Delta r$$

$$+ 2\pi\, r_j\, w^{l}_{j,k-(1/2)}\left(\rho^{l}_{j,k} - \rho^{l}_{j,k-(1/2)}\right)\Delta r = S(\rho)^{l}_{j,k}\, \delta_j - 2\pi\, r_j\, \rho^{l}_{j,k}\left(u^{l}_{j+(1/2),k} - u^{l}_{j-(1/2),k}\right)\Delta z$$

$$- 2\pi\, r_j\, \rho^{l}_{j,k}\left(w^{l}_{j,k+(1/2)} - w^{l}_{j,k-(1/2)}\right)\Delta r - 2\pi\, \rho^{l}_{j,k} \frac{u^{l}_{j+(1/2),k} + u^{l}_{j-(1/2),k}}{2} \Delta r\, \Delta z \qquad \text{(A2)}$$

It is shown in appendix B that space differences, such as those on the left-hand side of equation (A2), should be taken in the opposite direction from the local velocity vector. After noticing that the conservation properties of equation (A2) are not changed by cycling all the first or second subscripts of any term by the same amount, equation (A2) can be changed to

$$\delta_j \frac{\partial \rho^{l}_{j,k}}{\partial t} + a\, 2\pi\, r_j\, u^{l}_{j+(a/2),k}\left(\rho^{l}_{j+a,k} - \rho^{l}_{j,k}\right)\Delta z + b\, 2\pi\, r_j\, w^{l}_{j,k+(b/2)}\left(\rho^{l}_{j,k+b} - \rho^{l}_{j,k}\right)\Delta r$$

$$+ \pi\, u^{l}_{j+(a/2),k}\left(\rho^{l}_{j+a,k} - \rho^{l}_{j,k}\right)\Delta r\, \Delta z = S(\rho)^{l}_{j,k}\, \delta_j - 2\pi\, r_j\, \rho^{l}_{j,k}\left(u^{l}_{j+(1/2),k} - u^{l}_{j-(1/2),k}\right)\Delta z$$

$$- 2\pi\, r_j\, \rho^{l}_{j,k}\left(w^{l}_{j,k+(1/2)} - w^{l}_{j,k-(1/2)}\right)\Delta r - 2\pi\, \rho^{l}_{j,k} \frac{u^{l}_{j+(1/2),k} + u^{l}_{j-(1/2),k}}{2} \Delta r\, \Delta z \qquad \text{(A3)}$$

where a is sgn(-u) and b is sgn(-w). Equation (A3) was obtained from equation (A2) by cycling the j (or k) subscripts of the convective difference terms by ±1 so as to insure that each difference is taken in the opposite direction from the u (or w) velocity component.

The effects of the index cycling can be seen by noticing (for example) that cycling the k-index on convective differences taken in the z-direction in equation (A2) is equivalent to adding the term

$$-\pi\, r_j\, \Delta r\left[\left|w^l_{j,k+(1/2)}\right|\left(\rho^l_{j,k+1} - \rho^l_{j,k}\right) - \left|w^l_{j,k-(1/2)}\right|\left(\rho^l_{j,k} - \rho^l_{j,k-1}\right)\right]$$

to equation (A2). When this term is associated with the time derivative of density in equation (A2), there follows

$$\delta_j\left[\frac{\partial \rho^l_{j,k}}{\partial t} - \frac{\Delta z}{2}\,\frac{\left|w^l_{j,k+(1/2)}\right|\left(\rho^l_{j,k+1} - \rho^l_{j,k}\right) - \left|w^l_{j,k-(1/2)}\right|\left(\rho^l_{j,k} - \rho^l_{j,k-1}\right)}{\Delta z^2} + \text{Other terms}\right] = 0$$

Thus the term added for the z-direction (to obtain eq. (A3) from eq. (A2)) acts like the second-order differential operator in the classical heat-conduction equation and helps smooth irregularities in the density variations in the z-direction. Finally, divide equation (A3) by δ_j and get

$$\frac{\partial \rho^l_{j,k}}{\partial t} + a\, u^l_{j+(a/2),k}\,\frac{\rho^l_{j+a,k} - \rho^l_{j,k}}{\Delta r} + b\, w^l_{j,k+(b/2)}\,\frac{\rho^l_{j,k+b} - \rho^l_{j,k}}{\Delta z} + u^l_{j+(a/2),k}\,\frac{\rho^l_{j+a,k} - \rho^l_{j,k}}{2r_j}$$

$$= S(\rho)^l_{j,k} - \rho^l_{j,k}\,\frac{u^l_{j+(1/2),k} - u^l_{j-(1/2),k}}{\Delta r} - \rho^l_{j,k}\,\frac{w^l_{j,k+(1/2)} - w^l_{j,k-(1/2)}}{\Delta z}$$

$$- \rho^l_{j,k}\,\frac{u^l_{j+(1/2),k} + u^l_{j-(1/2),k}}{2r_j} \qquad \text{(A4)}$$

By virtue of its derivation, equation (A4) conserves mass in transit.

Consider next some quantity $Q^l_{j,k}$ which must be conserved in a time-integration scheme so that

$$\sum_{j,k}\left(\rho^{l+1}_{j,k}\, Q^{l+1}_{j,k}\right)\delta_j - \sum_{j,k}\left(\rho^l_{j,k}\, Q^l_{j,k}\right)\delta_j = \text{Constant} \qquad \text{(A5)}$$

which is identically equal to

$$\left[\sum_{j,k}\left(\rho_{j,k}^{l+1}\, Q_{j,k}^{l+1}\right)\delta_j - \sum_{j,k}\left(\rho_{j,k}^{l+1}\, Q_{j,k}^{l}\right)\delta_j\right] + \left[\sum_{j,k}\left(\rho_{j,k}^{l+1}\, Q_{j,k}^{l}\right)\delta_j - \sum_{j,k}\left(\rho_{j,k}^{l}\, Q_{j,k}^{l}\right)\delta_j\right] = \text{Constant} \qquad \text{(A6)}$$

If the time derivative of $\rho_{j,k}^{l}$ is taken to be

$$\frac{\partial \rho_{j,k}^{l}}{\partial t} = \frac{\rho_{j,k}^{l+1} - \rho_{j,k}^{l}}{\tau} \qquad \text{(A7)}$$

then equations (A6) and (A7) can be combined to get

$$\sum \delta\left[\frac{\partial\left(\rho_{j,k}^{l}\, Q_{j,k}^{l}\right)}{\partial t} - \rho_{j,k}^{l}\frac{\partial Q_{j,k}^{l}}{\partial t} - Q_{j,k}^{l}\frac{\partial \rho_{j,k}^{l}}{\partial t} - \tau\frac{\partial \rho_{j,k}^{l}}{\partial t}\frac{\partial Q_{j,k}^{l}}{\partial t}\right] = 0 \qquad \text{(A8)}$$

which shows that the finite-difference approximation for the differentiation of products is

$$\frac{\partial\left(\rho_{j,k}^{l}\, Q_{j,k}^{l}\right)}{\partial t} = \rho_{j,k}^{l}\frac{\partial Q_{j,k}^{l}}{\partial t} + Q_{j,k}^{l}\frac{\partial \rho_{j,k}^{l}}{\partial t} + \tau\frac{\partial \rho_{j,k}^{l}}{\partial t}\frac{\partial Q_{j,k}^{l}}{\partial t} \qquad \text{(A9)}$$

Finally, an approach similar to that used to derive equation (A4) can be applied to $Q_{j,k}^{l}$, which flows through δ_j, to find with the aid of equations (A4) and (A9) that

$$\rho_{j,k}^{l}\frac{\partial Q_{j,k}^{l}}{\partial t} + a\,\rho_{j+(a/2),k}^{l}\, u_{j+(a/2),k}^{l}\frac{Q_{j+a,k}^{l} - Q_{j,k}^{l}}{\Delta r} + b\,\rho_{j,k+(b/2)}^{l}\, w_{j,k+(b/2)}^{l}\frac{Q_{j,k+b}^{l} - Q_{j,k}^{l}}{\Delta z}$$

$$= S(\rho Q)_{j,k}^{l} - \tau\frac{\partial \rho_{j,k}^{l}}{\partial t}\frac{\partial Q_{j,k}^{l}}{\partial t} \qquad \text{(A10)}$$

Equation (A10) conserves $Q_{j,k}^{l}$ in transit.

APPENDIX B

RELATIONSHIP BETWEEN FINITE DIFFERENCES TAKEN AT CONSTANT TIME, AT CONSTANT SPACE POSITION, AND ALONG THE PARTICLE PATH

Equation (4) shows the relationship between derivatives taken at constant time, derivatives taken at constant space position, and derivatives taken along the particle path. In order to establish a finite-difference approximation for equation (4), consider a particle having a describing property Q and moving along a particle trajectory. A time difference taken at $\bar{r}$ is identically equal to

$$Q(\bar{r}, t+\tau) - Q(\bar{r},t) = \left[Q(\bar{r}, t+\tau) - Q(\bar{r}-\bar{\beta}, t)\right] + \left[Q(\bar{r}-\bar{\beta}, t) - Q(\bar{r},t)\right] \tag{B1}$$

so that

$$Q(\bar{r}, t+\tau) - Q(\bar{r}-\bar{\beta}, t) = \left[Q(\bar{r}, t+\tau) - Q(\bar{r},t)\right] + \left[Q(\bar{r},t) - Q(\bar{r}-\bar{\beta}, t)\right] \tag{B2}$$

where $\bar{\beta}$ is an arbitrary vector. Equation (B2) is a finite-difference relationship equivalent to equation (4). Thus the left-hand side of equation (B2) is a comoving difference. Since a particle trajectory which ends at $(\bar{r}, t+\tau)$ must begin at $(\bar{r}-\bar{V}\tau, t)$, where $\bar{V}$ is the local particle velocity, $\bar{\beta}$ must be equal to $\bar{V}\tau$. Denote the first difference in equation (B2) by $\Delta Q_{\text{trajectory}}$, the second difference by ΔQ_{time}, and the third difference by ΔQ_{space}. Take the limit of equation (B2) as τ goes to zero, and notice that $\frac{\Delta Q_{\text{space}}}{|\bar{\beta}|}$ usually is discontinuous at $\bar{r}$. The value of $\frac{\Delta Q_{\text{space}}}{|\bar{\beta}|}$ must be calculated from the space octant which contains the starting point of the particle trajectory that ends at $(\bar{r}, t+\tau)$. With this convention, equation (B2) becomes

$$\frac{\left[\Delta Q(\bar{r},t)\right]_{\text{trajectory}}}{\tau} \approx \frac{\left[\Delta Q(\bar{r},t)\right]_{\text{time}}}{\tau} + \frac{\Delta Q\left(\bar{r}-\frac{\bar{\beta}}{2}, t\right)_{\text{space}}}{|\bar{\beta}|}|\bar{V}| \tag{B3}$$

APPENDIX C

NUMERICAL STABILITY OF THE FREE-SURFACE EQUATIONS

The numerical stability study of the free-surface equations is made tractable by holding $\sigma^{l}_{j,k}$ constant in equations (25) and (26). Suppose u, w, and ϕ are known numerical solutions for the free-surface motions. Let U^{l}_{j}, W^{l}_{j}, and Φ^{l}_{j} be small space disturbances added to $u^{l}_{j,B}$, $w^{l}_{j,B}$, and ϕ^{l}_{j} in equations (18), (23), and (24). Neglect products of the small disturbance variables to find

$$U^{l+1}_{j} - U^{l}_{j} \approx -a\frac{\tau}{\Delta r}u^{l}_{j,B}\left(U^{l}_{j+a} - U^{l}_{j}\right) - a\frac{\tau}{\Delta r}\left(u^{l}_{j+a,B} - u^{l}_{j,B}\right)U^{l}_{j}$$

$$+\frac{\tau}{\rho^{l}_{j,B}}\frac{\partial\sigma^{l}_{j,B}}{\partial r}\left(\frac{\Phi^{l}_{j}}{z_k - \phi^{l}_{j}} + \frac{\Phi^{l}_{j+1} - \Phi^{l}_{j-1}}{\phi^{l}_{j+1} - \phi^{l}_{j-1}}\right) \tag{C1}$$

$$W^{l+1}_{j} - W^{l}_{j} \approx -a\frac{\tau}{\Delta r}u^{l}_{j,B}\left(W^{l}_{j+a} - W^{l}_{j}\right) - a\frac{\tau}{\Delta r}\left(w^{l}_{j+a,B} - w^{l}_{j,B}\right)U^{l}_{j}$$

$$+\frac{\tau}{\rho^{l}_{j,B}}\frac{\partial\sigma^{l}_{j,B}}{\partial z}\frac{\Phi^{l}_{j}}{z_k - \phi^{l}_{j}} \tag{C2}$$

and

$$\Phi^{l+1}_{j} - \Phi^{l}_{j} \approx -a\frac{\tau}{\Delta r}u^{l}_{j,B}\left(\Phi^{l}_{j+a} - \Phi^{l}_{j}\right) - a\frac{\tau}{\Delta r}\left(\phi^{l}_{j+a} - \phi^{l}_{j}\right)U^{l}_{j} + W^{l}_{j}\,\tau \tag{C3}$$

where a is sgn(-u). Next let

$$U^{l}_{j} = \sum_{n} A^{l}_{n}\, e^{in\gamma r} \tag{C4}$$

$$W^{l}_{j} = \sum_{n} B^{l}_{n}\, e^{in\gamma r} \tag{C5}$$

$$\Phi^{l}_{j} = \sum_{n} C^{l}_{n}\, e^{in\gamma r} \tag{C6}$$

APPENDIX C

$$\frac{\partial u}{\partial r} = a\,\frac{u^{l}_{j+a,B} - u^{l}_{j,B}}{\Delta r} \tag{C7}$$

$$\frac{\partial w}{\partial r} = a\,\frac{w^{l}_{j+a,B} - w^{l}_{j,B}}{\Delta r} \tag{C8}$$

$$\frac{\partial \phi}{\partial r} = a\,\frac{\phi^{l}_{j+a} - \phi^{l}_{j}}{\Delta r} \tag{C9}$$

$$u = u^{l}_{j,B} > 0 \tag{C10}$$

$$w = w^{l}_{j,B} \tag{C11}$$

$$\frac{1}{\rho}\frac{\partial \sigma}{\partial r} = \frac{1}{\rho^{l}_{j,B}}\frac{\partial \sigma^{l}_{j,B}}{\partial r} \tag{C12}$$

Substitute equations (C4) to (C12) into equations (C1) to (C3) to get for each value of n

$$A^{l+1}_{n} = A^{l}_{n} - \frac{\tau}{\Delta r}u\left(1 - e^{-in\gamma\Delta r}\right)A^{l}_{n} - \tau\frac{\partial u}{\partial r}A^{l}_{n} + \frac{\tau}{\rho}\frac{\partial \sigma}{\partial r}\left(\frac{1}{z_k - \phi^{l}_{j}} + \frac{2i\,\sin(n\gamma\Delta r)}{\phi^{l}_{j+1} - \phi^{l}_{j-1}}\right)C^{l}_{n} \tag{C13}$$

$$B^{l+1}_{n} = B^{l}_{n} - \frac{\tau}{\Delta r}u\left(1 - e^{-in\gamma\Delta r}\right)B^{l}_{n} - \tau\frac{\partial w}{\partial r}A^{l}_{n} + \frac{\tau}{\rho}\frac{\partial \sigma}{\partial z}\frac{1}{z_k - \phi^{l}_{j}}C^{l}_{n} \tag{C14}$$

and

$$C^{l+1}_{n} = C^{l}_{n} - \frac{\tau}{\Delta r}u\left(1 - e^{-in\gamma\Delta r}\right)C^{l}_{n} - \tau\frac{\partial \phi}{\partial r}A^{l}_{n} + B^{l}_{n}\,\tau \tag{C15}$$

These equations can be written in matrix form as

$$\begin{Bmatrix} A^{l+1}_{n} \\ B^{l+1}_{n} \\ C^{l+1}_{n} \end{Bmatrix} = \left[M(n,\tau)\right]\begin{Bmatrix} A^{l}_{n} \\ B^{l}_{n} \\ C^{l}_{n} \end{Bmatrix} \tag{C16}$$

where

$$M_{11} = 1 - \frac{\tau}{\Delta r}u\left(1 - e^{-in\gamma\Delta r}\right) - \tau\frac{\partial u}{\partial r}$$

$$M_{12} = 0$$

$$M_{13} = \frac{\tau}{\rho}\frac{\partial\sigma}{\partial r}\left(\frac{1}{z_k - \phi_j^l} + \frac{2i\,\sin(n\gamma\Delta r)}{\phi_{j+1}^l - \phi_{j-1}^l}\right)$$

$$M_{21} = -\tau\frac{\partial w}{\partial r}$$

$$M_{22} = 1 - \frac{\tau}{\Delta r}u\left(1 - e^{-in\gamma\Delta r}\right)$$

$$M_{23} = \frac{\tau}{\rho}\frac{\partial\sigma}{\partial z}\frac{1}{z_k - \phi_j^l}$$

$$M_{31} = -\tau\frac{\partial\phi}{\partial r}$$

$$M_{32} = \tau$$

$$M_{33} = 1 - \frac{\tau}{\Delta r}u\left(1 - e^{-in\gamma\Delta r}\right)$$

and $\left[M(n,\tau)\right]$ is called the amplification matrix. By repeated application of equation (C16),

$$\begin{Bmatrix} A_n^{l+1} \\ B_n^{l+1} \\ C_n^{l+1} \end{Bmatrix} = \left[M(n,\tau)\right]^l \begin{Bmatrix} A_n^1 \\ B_n^1 \\ C_n^1 \end{Bmatrix} \tag{C17}$$

Now let τ tend to zero in such a way that

$$\tau > 0$$

$$t = l\tau$$

$$l \to \infty$$

The integration scheme given by equation (C17) is said to be stable if and only if

$$\left|\left[M(n,\tau)\right]^l\{\mu\}\right| < \text{Constant} \tag{C18}$$

for any positive constant and l sufficiently large, where $\{\mu\}$ is an arbitrary unit vector and $|\ |$ indicates the norm.

APPENDIX C

If $\left[M(n,\tau)\right]$ can be written as

$$\left[M(n,\tau)\right] \leqq \left[M(n,0)\right] + \left[\text{Constant}\right]\tau \tag{C19}$$

as τ tends to zero, and if the largest eigenvalue of $\left[M(n,0)\right]$ is determined so that

$$\left|\lambda(m)\right| \leqq 1 \qquad (m = 1, 2, 3) \tag{C20}$$

then (see ref. 4) equation (C18) holds true. Equation (C19) is seen to hold by inspection of equation (C16). Furthermore, the eigenvalues of $\left[M(n,0)\right]$ are identical and equal to

$$\lambda(m) = 1 - \frac{\tau}{\Delta r} u\left(1 - e^{-in\gamma\Delta r}\right)$$

Thus if

$$\frac{\tau}{\Delta r} u \leqq 1 \tag{C21}$$

then $\left|\lambda(m)\right| \leqq 1$. Therefore equation (C17) is stable under numerical integration.

REFERENCES

1. Alder, Berni; Fernbach, Sidney; and Rotenberg, Manuel, eds.: Methods in Computational Physics. Vol. 3 – Fundamental Methods in Hydrodynamics. Academic Press, 1964.

2. Johnson, W. E.: OIL – A Continuous Two-Dimensional Eulerian Hydrodynamic Code. GAMD-5580-Revised (Contract DA-04-495-AMC-116(x)), Gen. Dyn. Corp., Jan 7, 1965. (Available from DDC as AD 477 240.)

3. Bjork, Robert L.: Review of Physical Processes in Hypervelocity Impact and Penetration. U.S. Air Force Proj. RAND Mem. RM-3529-PR, RAND Corp., July 1963.

4. Richtmyer, Robert D.: Difference Methods for Initial-Value Problems. Interscience Pub., Inc., 1957.

5. Tillotson, J. H.: Metallic Equations of State for Hypervelocity Impact. GA-3216 (Contract AF 29(601)-4759), Gen. Dyn., July 18, 1962.

"The aeronautical and space activities of the United States shall be conducted so as to contribute . . . to the expansion of human knowledge of phenomena in the atmosphere and space. The Administration shall provide for the widest practicable and appropriate dissemination of information concerning its activities and the results thereof."

— NATIONAL AERONAUTICS AND SPACE ACT OF 1958

NASA SCIENTIFIC AND TECHNICAL PUBLICATIONS

TECHNICAL REPORTS: Scientific and technical information considered important, complete, and a lasting contribution to existing knowledge.

TECHNICAL NOTES: Information less broad in scope but nevertheless of importance as a contribution to existing knowledge.

TECHNICAL MEMORANDUMS: Information receiving limited distribution because of preliminary data, security classification, or other reasons.

CONTRACTOR REPORTS: Scientific and technical information generated under a NASA contract or grant and considered an important contribution to existing knowledge.

TECHNICAL TRANSLATIONS: Information published in a foreign language considered to merit NASA distribution in English.

SPECIAL PUBLICATIONS: Information derived from or of value to NASA activities. Publications include conference proceedings, monographs, data compilations, handbooks, sourcebooks, and special bibliographies.

TECHNOLOGY UTILIZATION PUBLICATIONS: Information on technology used by NASA that may be of particular interest in commercial and other non-aerospace applications. Publications include Tech Briefs, Technology Utilization Reports and Notes, and Technology Surveys.

Details on the availability of these publications may be obtained from:

SCIENTIFIC AND TECHNICAL INFORMATION DIVISION

NATIONAL AERONAUTICS AND SPACE ADMINISTRATION

Washington, D.C. 20546